https://doi.org/10.5194/egusphere-2023-1152
Preprint. Discussion started: 16 June 2023

Subgridding High Resolution Numerical Weather Forecast in the Canadian Selkirk range for local snow modelling in a remote sensing perspective

Paul Billecocq[1, 2], Alexandre Langlois[1, 2], and Benoit Montpetit[3]

[1]Département de Géomatique appliquée, GRIMP, Université de Sherbrooke, Sherbrooke, QC, Canada
[2]Centre d'études nordiques, Québec, QC, Canada
[3]Climate Research Division, Environment and Climate Change Canada, Ottawa, ON, Canada

Correspondence: Paul Billecocq (paul.billecocq@usherbrooke.ca)

Abstract. Snow Water Equivalent (SWE) is a key variable in climate and hydrology studies. Current SWE products mask out high topography areas due to the coarse resolution of the satellite sensors used. The snow remote sensing community is hence pushing towards active microwaves approaches for global SWE monitoring. However, designing a SWE retrieval algorithm is not trivial, as multiple combinations of snow microstructure representations and SWE can yield the same radar signal. The community is converging towards forward modeling approaches using an educated first guess on the snowpack structure. Yet, snow highly varies in space and time, especially in mountain environments where the complex topography affects atmospheric and snowpack state variables in numerous ways. Automatic Weather Stations (AWS) are too sparse, and high-resolution Numerical Weather Predictions systems have a maximal resolution of 2.5 km × 2.5 km, which is too coarse to capture snow spatial variability in a complex topography. In this study, we designed a subgridding framework for the Canadian High Resolution Deterministic Prediction System. The native 2.5 km × 2.5 km resolution forecast was subgridded to a 100 m × 100 m resolution and used as the input for snow modeling over two winters in Glacier National Park, British Columbia, Canada. Air temperature, relative humidity, precipitation and wind speed were first parameterized regarding elevation using six Automatic Weather Stations. Alpine3D was then used to spatialize atmospheric parameters and radiation input accounting for terrain reflections and perform the snow simulations. Modeled snowpack state variables relevant for microwave remote sensing were evaluated against profiles generated with Automatic Weather Stations data and compared to raw HRDPS driven profiles. Overall, the subgridding framework improves the optical grain size (OGS) bias by 0.04 mm, the density bias by 2.7 $kg \cdot m^{-3}$ and the modelled SWE by 17% (up to 41% in the best case scenario). Overall, this work provides the necessary basis for SWE retrieval algorithms using forward modeling in a Bayesian framework.

1 Introduction

Seasonal snow governs several feedback loops that directly affect our planet's climate and plays a major role in its hydrological dynamics. With its high albedo, snow reflects a large proportion of the incoming solar radiation, which in return helps to mitigate global warming (IPCC, 2019). Furthermore, snow insulates the underlying soil, affecting the microbial activity, carbon

https://doi.org/10.5194/egusphere-2023-1152
Preprint. Discussion started: 16 June 2023

fluxes, and permafrost freeze/thaw cycles (Natali et al., 2019; Biskaborn et al., 2019). Moreover, seasonal snow melt provides connected watersheds with freshwater, sustaining natural ecosystems and human infrastructure . Finally, extreme precipitation events and resulting snow melt can cause devastating floods (Pomeroy et al., 2016; Vionnet et al., 2020), so that managing runoff would highly benefit both society and the economy (Sturm et al., 2017).

Yet, snow mass (or Snow Water Equivalent, SWE) remains poorly characterized, especially in mountainous regions where a significant amount of SWE is stored at the continent scale (Wrzesien et al., 2018). Global SWE products inferred from passive microwave observations are available at a 25 km resolution (Luojus et al., 2021), which is too coarse to capture the SWE spatial variability (Derksen et al., 2021), and mountains are simply omitted or masked out. Moreover, both observations from passive microwaves and modeling efforts yield negative biases when estimating mountain or deep-snow SWE (Vuyovich et al., 2014; Wrzesien et al., 2018; Pulliainen et al., 2020). Hence, the snow remote sensing community is promoting active remote sensing, which provides higher spatial resolution information compared to passive microwaves products (Tsang et al., 2022; Rott et al., 2010; Derksen et al., 2021). The sensitivity of the Synthetic Aperture Radar (SAR) signal to SWE has been proven at the Ku-band (King et al., 2015; Lemmetyinen et al., 2016), and recent studies suggest that C-band could also be used for snow depth retrieval (Lievens et al., 2019, 2022), a key parameter for SWE retrieval, although it is contrasting with previous research (Dozier and Shi, 2000). However, linking SWE to SAR backscattering is not trivial as it does not depend solely on SWE (which is a function of snow height and density), but also on the snow microstructure. Consequently, several combinations of SWE and snowpack microstructures can yield similar backscattering values, creating a non-unique inversion solution (Tsang et al., 2022). As a result, recent inversion algorithms tend towards a Bayesian framework where a forward scattering model is used to generate possible backscattering values, and the best fitting one is selected using a weighted cost function (Lemmetyinen et al., 2018; King et al., 2018, 2019; Zhu et al., 2021). So far, these studies only paired airborne radar observations with fields measurements, but coupling a radiative transfer model with a snow physics model still has to be explored in the active microwaves domain.

Advanced thermodynamic multi-layered snow models such as Crocus or SNOWPACK produce SWE and microstructure parameters estimates (Brun et al., 1992; Vionnet et al., 2012; Lehning et al., 2002). Such models can be driven either by Automatic Weather Stations (AWS) measurements, atmospheric models, or reanalysis products. On the one hand, weather stations provide very accurate measurements of the atmospheric conditions at the local scale. However, they need human maintenance, are subject to outages and local biases, and as a result, AWS spatial interpolation in complex terrain is not always accurate (Lundquist et al., 2019). On the other hand, high-resolution atmospheric models are known for their negative bias in precipitation, resulting in a negative bias in snow depth and SWE (Bellaire et al., 2011, 2013; Côté et al., 2017). Moreover, their spatial resolution (2.5–3 km) is too coarse to represent properly the spatial variability of atmospheric parameters and snow properties in complex terrain (Grünewald et al., 2010; Vionnet et al., 2021). Vionnet et al. (2021) developed a downscaling scheme for the High-Resolution Deterministic Prediction System (HRDPS, Milbrandt et al. (2016)) to feed a snowdrift-permitting snowpack model. However, this study was focused on accurately modeling snow redistribution processes (e.g., wind transport and avalanches) using the two-layer snow model Snobal in which the snow microstructure representation is not precise enough for forward radiative transfer modeling.

https://doi.org/10.5194/egusphere-2023-1152
Preprint. Discussion started: 16 June 2023

To our knowledge, downscaling Numerical Weather Predictions in complex terrain to improve modeling of snow SAR remote sensing retrieval parameters, namely SWE and microstructure, remains unresolved. This research thus aims to develop and evaluate a novel downscaling framework for the atmospheric HRDPS model over broad mountainous regions. First, we downscaled gridded atmospheric parameters as a Virtual Weather Station array using a novel strategy combining both statistical and physical approaches. Second, we spatialized atmospheric parameters and performed snow simulations on the study area using the Alpine3D model (Lehning et al., 2006) over two consecutive winters (2018–2019 and 2019–2020). Weather parameters subgridding and snowpack state parameters were assessed at three reference weather stations using an array of statistical criteria and a Dynamic Time Warping algorithm (Hagenmuller and Pilloix, 2016; Hagenmuller et al., 2018; Herla et al., 2021). Finally, we assessed the spatial variability capacity of the proposed subgridding framework within one HRDPS grid cell.

2 Study area

This study was conducted in Glacier National Park (GNP), British Columbia, Canada (Figure 1), which is part of the Selkirk range in the Columbia Mountains. The study area is 18 km by 16 km wide, covering 288 km^2 of complex topography, with elevations ranging from 840 m a.s.l at the valley bottom to 3284 m a.s.l. In winter, the Columbia Mountains snowpack is characterized as a transitional snowpack with a maritime influence. Hence, westerly fluxes coming from the Pacific mainly govern the precipitation pattern in this mountain range. Occasionally, dryer and colder systems from the northeast can also hit the range, bringing some continental influence to the east of the study area. On average, the snowpack reaches 3.2 m at its peak, usually around the end of March and early April.

The Park has seven Automatic Weather Stations (AWS) at different elevations around the Highway corridor. The measured variables are air temperature (TA, °C), relative humidity (RH, %), wind speed (VW, $m.s^{-1}$), wind direction (DW, degrees), precipitation (PSUM, mm), incoming long wave radiation (ILWR, $W.m^{-2}$) and incoming shortwave radiation (ISWR, $W.m^{-2}$). Some stations include a snow height (HS, cm) sensor. Table 1 summarizes the set of meteorological variables available for each AWS. In this study, we used two winter time series: from September to April, 2018–2019 and 2019–2020. The 2018–2019 season had overall colder temperatures and was relatively dry. The 2019–2020 season had milder temperatures and abundant precipitations. As a result, in 2019–2020, the snowpack was deeper and mostly composed of round grains where, in 2018–2019, the shallower snowpack and colder temperatures led to a mostly faceted snowpack. Both seasons had rain-on-snow episodes in the early season, which created melt-freeze crusts at the bottom of the snowpack.

3 The Numerical Weather Predictions downscaling processing chain design

Figure 2 summarizes the Numerical Weather Predictions (NWP) downscaling processing chain.

https://doi.org/10.5194/egusphere-2023-1152
Preprint. Discussion started: 16 June 2023

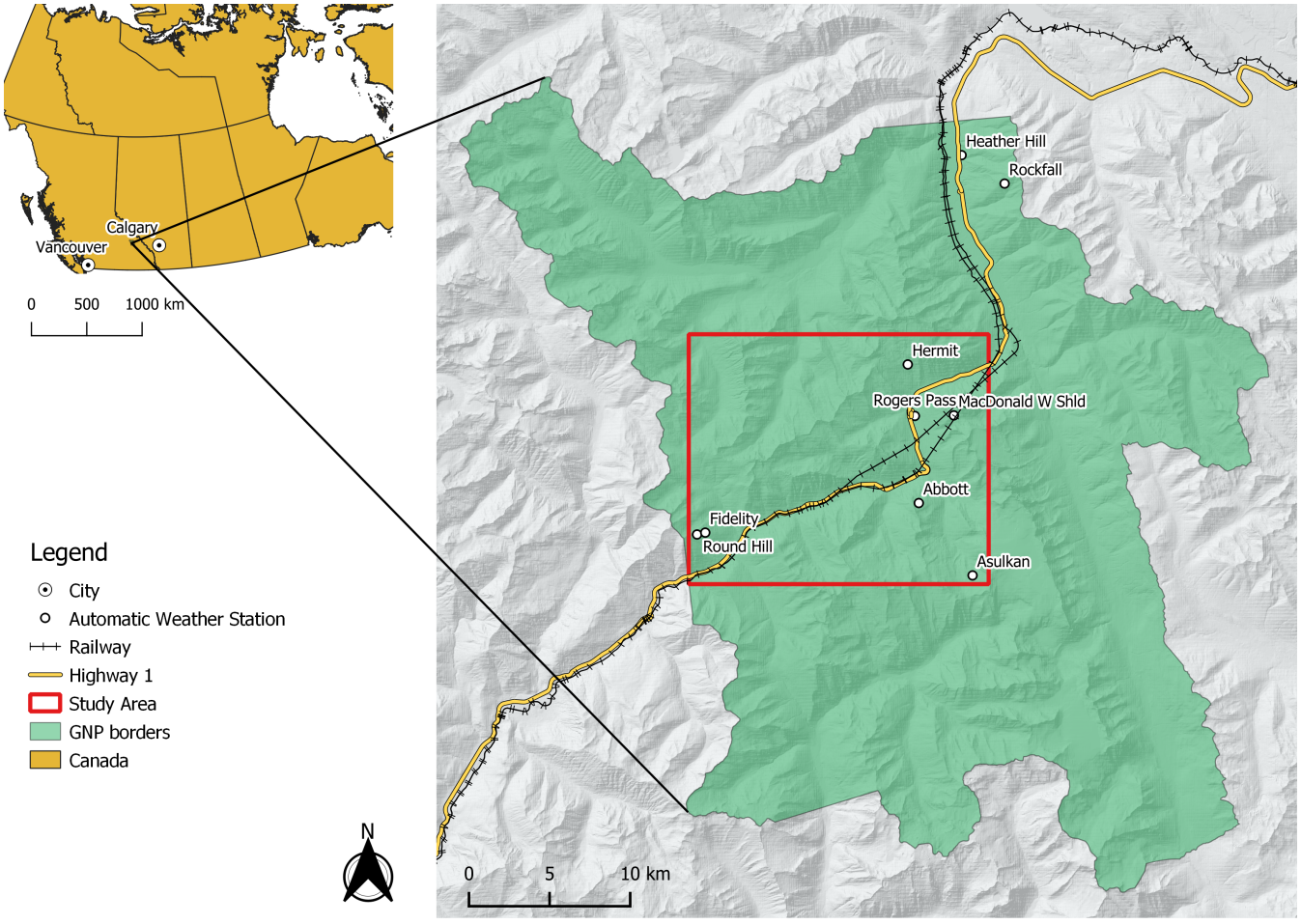

Figure 1. Glacier National Park, British Columbia, Canada

Weather station	Elevation	TA	RH	VW	DW	PSUM	ILWR	ISWR	HS
Abbott	2085 m	X	X	X	X	X			X
Hermit	1950 m	X	X	X	X	X			X
Fidelity	1905 m	X	X	X	X	X	X	X	X
McDonad W shoulder	1930 m	X	X	X	X				
Rogers Pass	1315 m	X	X	X	X	X			X
Round Hill	2100 m	X	X	X	X	X			

Table 1. Weather stations characteristics

https://doi.org/10.5194/egusphere-2023-1152
Preprint. Discussion started: 16 June 2023

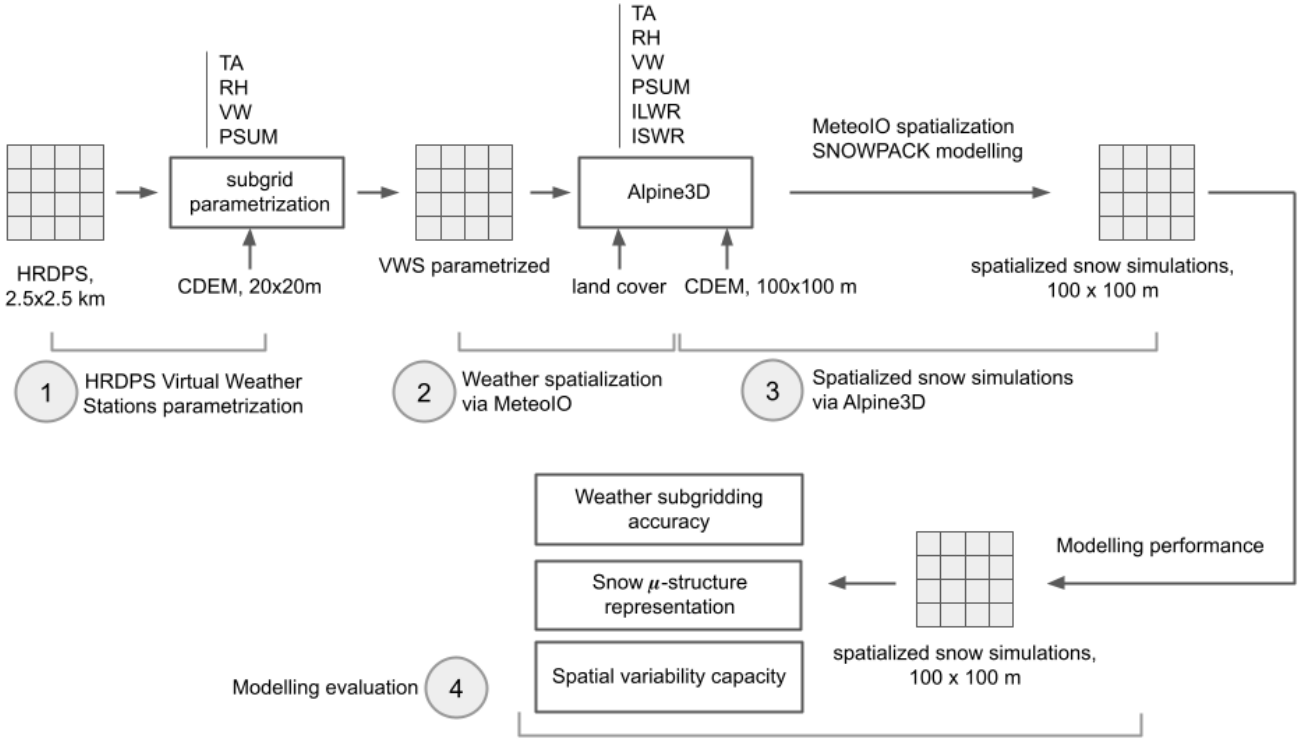

Figure 2. Numerical Weather Predictions downscaling scheme flowchart

3.1 HRDPS subgridding and Alpine3D simulations

The High Resolution Deterministic Prediction System (HRDPS) produced by the Meteorological Service of Canada provides a 2.5 km gridded hourly forecast of atmospheric variables for most of Canada (Milbrandt et al., 2016). Atmospheric variables are computed for each pixel at a reference elevation provided by the underlying 2.5 km resolution Digital Elevation Model. This study is based on a grid composed of 70 HRDPS prediction cells overlying the study area, and including the following variables: TA, RH, VW, DW, PSUM, ISWR, and ILWR. First, using the 20 m Canadian Digital Elevation Model (CDEM), we transformed each HRDPS cell data into a Virtual Weather Station. To do so, each cell centroid coordinates was recomputed, minimizing the hypotenuse distance between each underlying CDEM pixel centroid and the HRDPS centroid, in an 800 m radius around the original HRDPS centroid. Then, TA, RH and PSUM were parameterized to correct for the model's biases and account for the elevation discrepancy between the HRDPS cell elevation and the new centroid CDEM elevation. Finally, VW was parameterized to account for the topography underlying the 2.5 km resolution grid unresolved by HRDPS.

Bias in air temperature was found to have a non-linear relationship with the elevation difference between the station elevation and the original HRDPS cell elevation. We designed a logarithmic regression fit to compute the TA bias as a function of

https://doi.org/10.5194/egusphere-2023-1152
Preprint. Discussion started: 16 June 2023

elevation difference, and applied it when the elevation difference was over 100 m.

$$\mathrm{TA}_p = \begin{cases} \mathrm{TA}_{hrdps} + ln(-0.012\Delta_E + 6.89) & \text{if } |\Delta_E| > 100 \\ \mathrm{TA}_{hrdps} & \text{otherwise} \end{cases} \quad (1)$$

where:

Δ_E corresponds to the elevation difference between the CDEM cell and the HRDPS cell, TA_p is the parameterized air temperature, and TA_{hrdps} is the raw HRDPS air temperature.

RH was corrected by first converting relative humidity to dew point temperature, as described in Liston and Elder (2006). This dew point temperature was then adjusted using the logarithmic fit presented above, and converted back to relative humidity.

Snow precipitation water equivalent was first parameterized using an elevation lapse-rate correction. This lapse rate was computed using four weeks of manual SWE measurements on four conventional HN24 precipitation boards placed between 1330 m and 1920 m at Mt Fidelity.

$$\mathrm{PSUM}_p = \mathrm{PSUM}_{hrdps} + 0.0011 \times \Delta_E \times \mathrm{PSUM}_{hrdps} \quad (2)$$

Finally , the HRDPS VW was downscaled to the 20 m CDEM resolution at each new centroid position, as per the method described in Helbig et al. (2017). First, the coarse-scale surface wind is parameterized to account for underlying topography unresolved by HRDPS using the Sky View Factor parameter F_{sky}. The Sky View Factor is derived from the mean squared slope μ, and the typical length of topographic features ξ.

$$\mu = \left[\frac{\overline{(\partial_x z)^2 + (\partial_y z)^2}}{2}\right]^{1/2} \equiv \mu = \frac{\overline{[(z_{i,j} - z_{i+1,j})^2 + (z_{i,j} - z_{i,j+1})^2]}^{1/2}}{\Delta x\sqrt{2}} \quad (3)$$

$$\xi = \frac{\sigma_{DEM}\sqrt{2}}{\mu} \quad (4)$$

$$F_{sky}(L/\xi, \mu) = \left(1 - \left(1 - \frac{1}{(1 + a\mu^b)^c}\right)e^{-d(L/\xi)^{-2}}\right) \quad (5)$$

where:

a, b, c, and d are scaling coefficients, with a = 3.354688, b = 1.998767, c = 0.20286, and d = 5.951. L is the coarse-scale cell size, Δ_x is the subgrid cell size, and σ_{DEM} is the typical valley to peak elevation difference, e.g., the elevation standard deviation within each coarse resolution cell.

The coarse-scale VW is parameterized using the following relationship:

$$\mathrm{VW}_p = \mathrm{VW}_{hrdps}.F_{sky}(L/\xi, \mu) \quad (6)$$

Finally, VW_p is subgridded by applying a topographic downscaling factor $X^{dsc}_{topo}(\nabla^2 z, \mu)$ specific to each subgrid cell, based on the mean squared slope parameter μ, and a parameter related to the elevation laplacian $\nabla^2 z$.

$$\nabla^2 z = \nabla^2 z'.\frac{\Delta_x}{4} \quad (7)$$

https://doi.org/10.5194/egusphere-2023-1152
Preprint. Discussion started: 16 June 2023

and

$$\nabla^2 z' = \Big(z(x-\Delta x,y) + z(x+\Delta x,y) + z(x,y-\Delta x) + z(x,y+\Delta x) - 4z(x,y)\Big)/\Delta x^2 \quad (8)$$

The topographic downscaling factor is then computed as:

$$X_{topo}^{dsc}(\nabla^2 z, \mu) = \Big(1 - \frac{a'\nabla^2 z}{1 + a'|\nabla^2 z|^{b'}}\Big)\frac{c'}{1 + d'\mu^{e'}} \quad (9)$$

where:

$a' = 17.0393$, $b' = 0.737$, $c' = 1.0234$, $d' = 0.3794$, and $e' = 1.9821$.

Finally, the subgridded surface wind VW_{dsc} is obtained by applying the following relationship:

$$\mathrm{VW}_{dsc} = \mathrm{VW}_p . X_{topo}^{dsc}(\nabla^2 z, \mu) \quad (10)$$

These Virtual Weather Stations were then spatially interpolated on a 100 m grid via MeteoIO (Bavay and Egger, 2014) using the CDEM grid resampled to 100 m. TA was spatialized using a simple lapse rate computed from the AWS data and Inverse Distance Weighting (IDW). RH, VW, and DW were spatialized using the Micromet algorithms described in Liston and Elder (2006). To spatialize precipitations, we used topographic parameters and prevailing winds to alter the precipitation field, to account for wind snow redistribution (Winstral et al., 2002). Incoming shortwaves were spatialized considering terrain shading, slopes and reflections from neighboring cells. Finally, ILWR was spatialized using IDW. All the algorithms mentioned above are a part of the MeteoIO library, which is integrated into the Alpine3D model (Lehning et al., 2006).

Alpine3D is a spatially distributed 3D model, which allows running the vertical 1D snow model SNOWPACK over an area, considering the spatial processes affecting atmospheric variables(Bartelt and Lehning, 2002; Lehning et al., 2002, 2006). The model was run at Rogers Pass on the same 100 m grid described above, over an area of 18 km × 16 km (288 km^2) centered on the Highway 1 corridor for winters 2018–2019 and 2019–2020. We generated outputs for three reference stations: Fidelity, Hermit, and Abbott. To assess the spatial variability capacity of the subgridding framework, we also generated outputs at six points within the same cell. Elevation in the chosen cell ranges from 1470 m to 2566 m, and no glacier is present in the area. Three points are located on north-facing slopes, three points on south facing slopes, and one point per elevation band for each aspect (Below Treeline, z <1850 m; Treeline, 1850 m <z <2150 m; Alpine, z >2150 m).

3.2 Validation data and atmospheric parameters subgridding evaluation

To validate the HRDPS—Alpine3D snow simulations on the two winter datasets, we performed SNOWPACK simulations driven with AWS data at Fidelity, Hermit and Abbott stations. We filtered weather station data to remove outliers; data gaps smaller than six hours were linearly interpolated while larger gaps were filled using parameterized HRDPS data. Note that the Abbott station is located in a thunderstorms-prone area. Hence, the station is shut down all summer and is only turned back on mid-October. Parameterized HRDPS data are again used to fill in this gap.

The Numerical Weather Forecast subgridding quality was statistically assessed using three well-known criteria: bias, Mean

https://doi.org/10.5194/egusphere-2023-1152
Preprint. Discussion started: 16 June 2023

Absolute Error (MAE), and Spearman R correlation coefficient. These indicators allowed to quantify respectively the systematic difference between the models and the ground-truth measurements at the AWS, the prediction accuracy, and the strength of the association between modeled variables and the ground truth. To smooth small time lags between modeled meteorological events and measurements at the AWS, we averaged the meteorological time series over 2-hour time steps, and reaccumulated precipitations over the same period.

3.3 Snow modeling evaluation

Dynamic Time Warping (DTW) is an algorithm developed to measure the similarity between two sequences. In a nutshell, DTW computes the optimal match between two signals, while allowing for an elasticity in time (or space, in the case of snow profiles). It first resamples the two sequences on 1D-grids of the same elemental size and length. Then, a local cost matrix $\boldsymbol{D}$ is built, summarizing the distance between every elemental pair. From there, an accumulated cost matrix $\boldsymbol{G}$ is built by computing the accumulated cost to iterate from one element of $\boldsymbol{D}$ to the next one, respecting a predefined constraint set. The optimal alignment is found by minimizing the alignment accumulated cost.

Although originally designed for speech recognition (Sakoe and Chiba, 1978), DTW is extensively used in time series analysis, and it has recently received an increased interest by the snow community (Hagenmuller and Pilloix, 2016; Hagenmuller et al., 2018; Viallon-Galinier et al., 2020; Herla et al., 2021). In the snow science community, DTW has only been used so far in an avalanche forecasting perspective, focusing on aligning standard snow parameters (e.g., grain type, hardness, Liquid Water Content). In this study, we present a new development to the open-source DTW snow profile alignment package written by Herla et al. (2021), allowing to align snow profiles on remote sensing-oriented snow parameters, namely, layer density and Optical Grain Size (OGS), two key parameters in snow radiative transfer modeling. To do so, an alternative cost function was added to compute the local cost matrix $\boldsymbol{D}$.

$$D_{i,j} = w_d d_d(q_i^d, r_j^d) + w_{ogs} d_{ogs}(q_i^{ogs}, r_j^{ogs}) \tag{11}$$

where w_d and w_{ogs} are averaging weights respectively applied to density and OGS ($w_d + w_{ogs} = 1$), r_n^k denotes the n^{th} element of the reference profile $\boldsymbol{R}$, and q_n^k denotes the n^{th} element of the query profile $\boldsymbol{Q}$. Finally, $d_d()$ and $d_{ogs}()$ correspond to the distance function for density and OGS respectively, which is simply the absolute difference between the two elements, normalized over the entire vertical profile.

The space elasticity in the alignment algorithm allows to find the best match for a layer of the query profile in the same depth range in the reference profile. The algorithm constraints define the amount of elasticity allowed, i.e., the warping window definition and the local slope constraint. These constraints are essential to keep the algorithm from degenerating and generate irrelevant alignments. However, atmospheric models tend to strongly underestimate precipitations in mountain environments (Bellaire et al., 2011, 2013; Côté et al., 2017). Hence, profiles generated from atmospheric models and ground truth profiles can have a significant difference in HS. Physically matching layers are then too far apart, according to the algorithm's constraints, preventing the algorithm from generating relevant matches. Therefore, we artificially inflated profiles modeled using NWP, each layer being multiplied by the height ratio with the station profile. This allowed to rely solely on snow microstructure

https://doi.org/10.5194/egusphere-2023-1152
Preprint. Discussion started: 16 June 2023

parameters for the alignment, assessing only the microstructure representation. The generated aligned (or warped) profile was then used to compute a mean layer-by-layer bias for density and OGS with respect to the ground truth. For more details on the DTW implementation used in this paper, please refer to Herla et al. (2021). Height of Snow and SWE were visually assessed, and the Nash-Sutcliffe model efficiency coefficient (Nash and Sutcliffe, 1970) allowed to assess the SWE modeling quality using HRDPS and subgridded HRDPS data versus the station runs over the two seasons. The Nash-Sutcliffe model efficiency coefficient (NSE) is computed as:

$$NSE = 1 - \frac{\sum_{t=1}^{T}(y_{obs}^{t} - y_{model}^{t})^2}{\sum_{t=1}^{T}(y_{obs}^{t} - \overline{y_{obs}})^2} \tag{12}$$

4 Results

4.1 Numerical Weather Forecast subgridding performance

Figure 3 summarizes the performances of the subgridding framework (denoted as SGF in the figures) applied to the 2018–2019 and 2019–2020 HRDPS time series. The framework delivers a mixed performance for TA in 2018–2019. The HRDPS model shows a 1.6 °C bias at Abbott, which is reduced by approximately 1 °C using the subgridding framework. However, the positive bias is increased by 0.5 °C at the Fidelity station and very slightly at Hermit station (<0.5 °C). On the other hand, the Mean Absolute Error (MAE) and the Spearman R coefficient are slightly increased for most of the validation stations. TA shows a very strong correlation with station measures (R>0.8).

Relative Humidity subgridding yields good performances where the HRDPS model bias and MAE are reduced by 1% to 5% in most cases. The bias is constant at Fidelity station, as is the MAE at Abbott. The Spearman correlation coefficient is also slightly increased at Hermit and Fidelity stations and only shows a slight decrease at Abbott. Finally, modeled RH shows a strong correlation with station values (0.6 <R <0.8).

Overall, the framework performs best at subgridding VW. HRDPS is constantly overestimating wind speed by 1.5 $m.s^{-1}$. This bias is considerably reduced to 0.25 $m \cdot s^{-1}$ on average, and MAE is reduced by around 1 $m.s^{-1}$. However, the correlation with station values is overall weak (0.2 <R <0.4), and the subgridding workflow seems to have even weakened this correlation, except for Hermit station, which shows a negligible correlation (R <0.2).

Finally, subgridding shows good performance for PSUM as well. In agreement with the literature, the bias in modeled precipitation shows a general lack of precipitation in the HRDPS model, and ranged from 0.05 mm to 0.15 mm. MAE values range between 0.25 mm and 0.35 mm. With the subgridding, these values decrease at Abbott, increase slightly at Hermit, and stay constant at Fidelity. Correlation with station values is moderate at Abbott and Hermit (0.4 <R <0.6) and strong at Fidelity (0.6 <R <0.8). Finally, subgridding slightly improves the correlation with AWS measurements at the former sites and stayed constant at the latter. For 2019–2020, the results are very similar to the 2018–2019 season; the bias and MAE are corrected on the same scale and the Pearson R coefficient is on the same range for each variable. The only notable difference is that the PSUM bias at Abbott is negative for this season, meaning that HRDPS overestimated precipitations, which is highly unusual. As a result, the subgridding framework introduces even more precipitation bias (+ 0.07 mm).

https://doi.org/10.5194/egusphere-2023-1152
Preprint. Discussion started: 16 June 2023

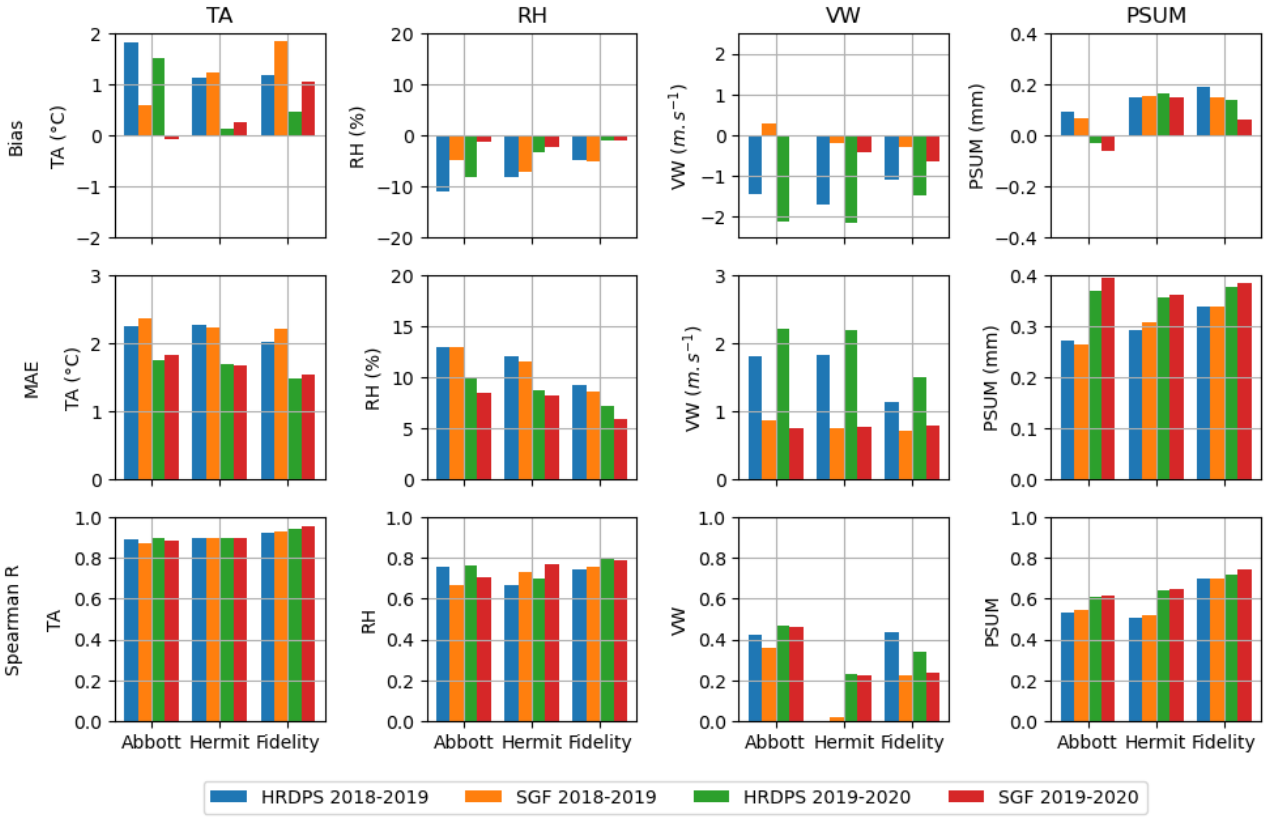

Figure 3. Atmospheric parameters evaluation for seasons 2018–2019 and 2019–2020.

4.2 Subgridding performance for snow modeling

Figures 4 and 5 summarize the subgridding framework performances for seasons 2018–2019 and 2019–2020. For 2018–2019, snowpack similarity shows the same behavior at every site and for both HRDPS and the subgridding framework. The season begins with average similarity values (around 0.5), then it plummets to low values in mid-October (<0.5) before improving to higher levels of similarity in November and for the rest of the season (0.6 <sim <0.8). In general, HRDPS simulations tend to have a better similarity with the AWS driven SNOWPACK simulations early in the season. The subgridded profiles tend to score higher similarities than HRDPS profiles in the mid-season before converging back with HRDPS in the spring. For the 2019–2020 season, similarity is again highly variable around 0.5 at Abbott and Hermit for both HRDPS and the subgridding framework. The early season at Fidelity shows very low similarities for the subgridding framework and HRDPS respectively. Then, starting in November, the similarities stabilize and slowly rise throughout the season to 0.8 at every site. Again, the subgridding framework shows a higher similarity than HRDPS during the mid-winter period at Abbott and Hermit. HRDPS reaches the same level of similarity by early spring or the end of the winter, respectively. At Abbott, the HRDPS and subgridding framework similarities are very similar, though HRDPS shows more fluctuations during most of the winter and early

https://doi.org/10.5194/egusphere-2023-1152
Preprint. Discussion started: 16 June 2023

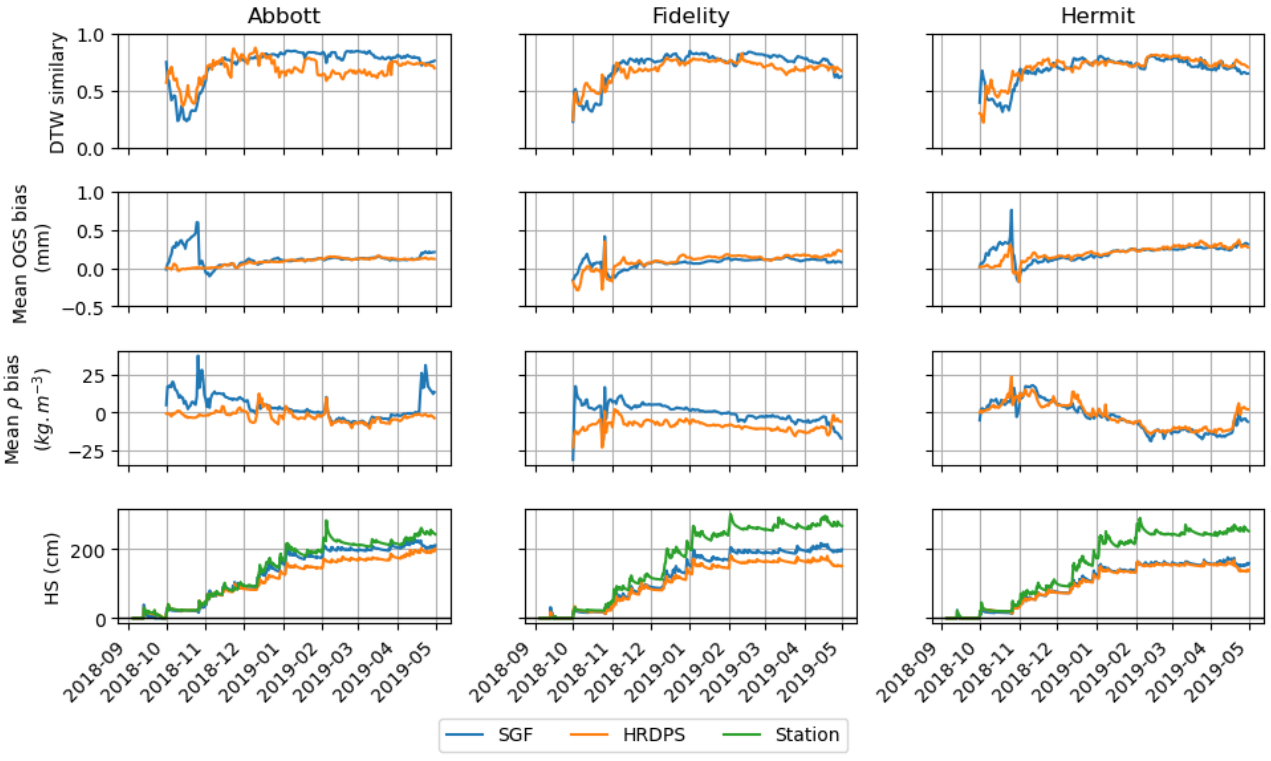

Figure 4. Snowpack similarity assessment for season 2018–2019

spring. The average similarity for all sites and seasons is 0.73 for the subgridding framework and 0.70 for the HRDPS profiles. Overall, the subgridding framework increased snowpack similarity by 2% at Abbott, by 1% at Hermit, and by 4% at Fidelity. The mean layer-by-layer error in OGS shows a similar behaviour to similarity at every site in 2018–2019 for both approaches. The error peaks and fluctuates strongly in the early season for both approaches, then stabilizes around mid-November. Considering the high variability in the fall for both seasons (September to November included), the first three months were considered as a spin-up phase for the model to initiate a proper snowpack. Hence, the numerical analysis of the results was carried out starting on the first of December. Both HRDPS and the subgridding framework are slightly overestimating OGS, but overall, the proposed method allows decreasing the bias by 0.03 mm at Fidelity and 0.02 mm at Hermit. However, OGS bias increased by 0.01 mm at Abbott on the same period. The same pattern repeats for the 2019–2020 season at all sites, where the subgridding framework decreases on average the OGS bias by 0.01 mm at Abbott, 0.09 mm at Fidelity and 0.08 mm at Hermit.

Similarly to OGS, in 2018–2019, the mean layer-by-layer error in density shows higher values in the early season, and stronger fluctuations for both HRDPS and the subgridding framework. Variations tend to stabilize by mid-November, and the error increases again towards the end of the season. Again, the numerical analysis was performed from the first of December until the end of the simulation for both seasons. Generally, the HRDPS model seems to underestimate snow density. The proposed framework brought on average a $2.58 kg \cdot m^{-3}$ improvement at Abbot and a $7.25 kg \cdot m^{-3}$ improvement at Fidelity for

https://doi.org/10.5194/egusphere-2023-1152
Preprint. Discussion started: 16 June 2023

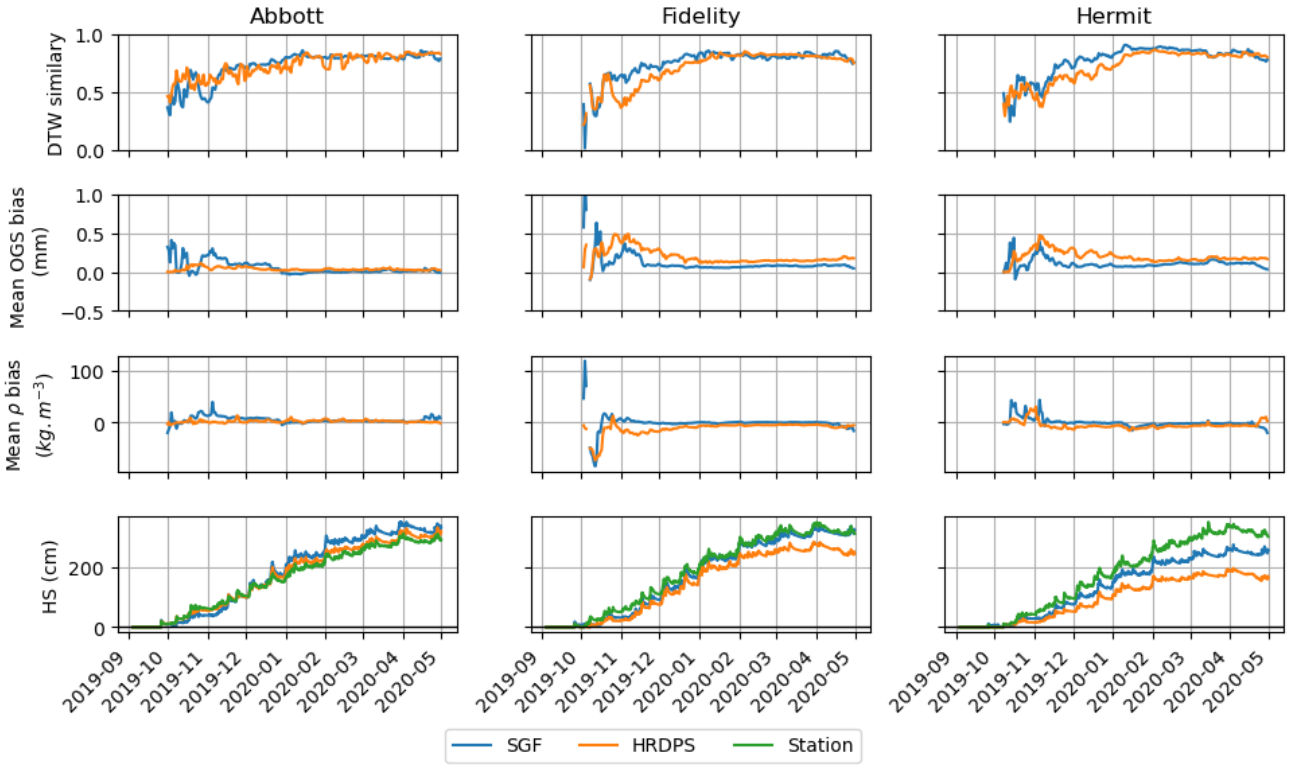

Figure 5. Snowpack similarity assessment for season 2019–2020

the 2018–2019 season. However, on the same period at Hermit, the density bias increased by $2.12kg \cdot m^{-3}$ on average. In 2019–2020, the density bias decreased on average by $5.44kg \cdot m^{-3}$ at Fidelity and $4.05kg \cdot m^{-3}$ at Hermit. However, the density bias increased by $0.9kg \cdot m^{-3}$ over the same period at Abbott.

Finally, the framework improves the modeled HS by 55 cm on average in 2018–2019, and by 35 cm on average in 2019–2020. However, HRDPS overestimated PSUM at Abbott in 2019–2020, which resulted in overestimating HS. As a result, the subgridding framework overestimated HS even more for this case, which inflates the overall HS mean error for the season. Finally, HS remained relatively unchanged at Hermit for 2018–2019 as the framework did not bring a substantial improvement.

Overall SWE modeling was considerably improved at all stations except at Abbott in 2019–2020 (Figure 6). Table 2 summarizes the Nash Sutcliffe Efficiency coefficient (NSE) values at each site and for each season. On average, the subgridding framework improves the SWE NSE by 17%, and by 41% at Hermit in 2018–2019.

4.3 Spatial variability representation capacity

Figure 7 summarizes the main atmospheric parameters values for the six spatial variability sites, averaged per month (and accumulated for precipitations). First, the subgridding framework creates a realistic altitudinal temperature gradient, temperatures

https://doi.org/10.5194/egusphere-2023-1152
Preprint. Discussion started: 16 June 2023

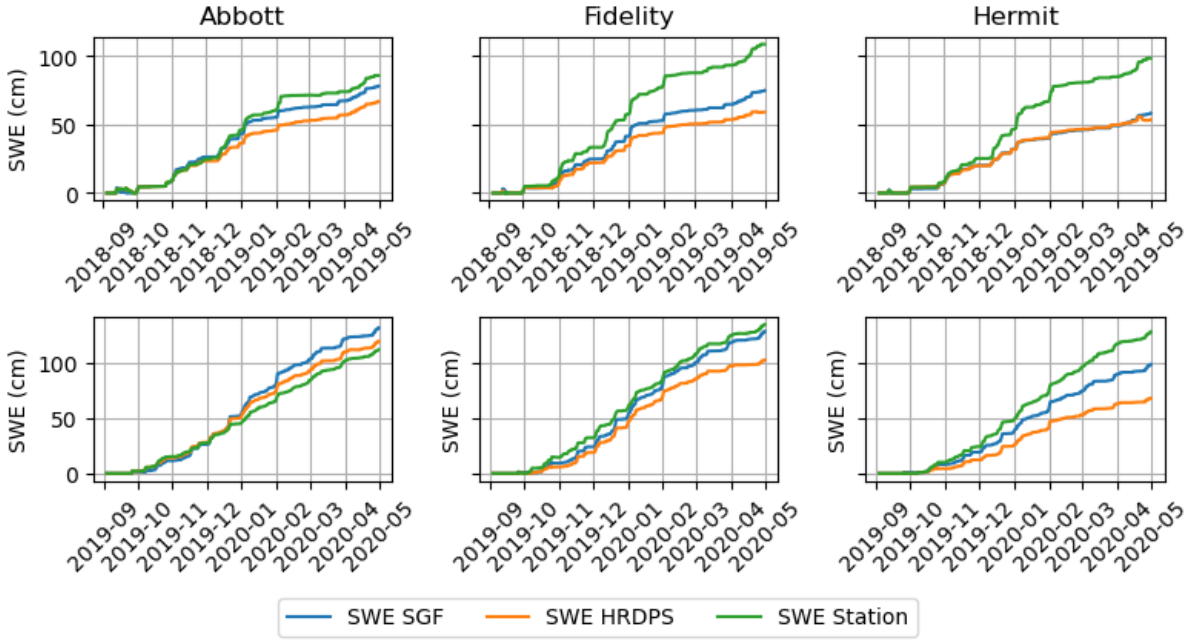

Figure 6. SWE modeling for seasons 2018–2019 and 2019–2020

	Abbott		Fidelity		Hermit	
	2018-2019	2019–2020	2018-2019	2019–2020	2018-2019	2019–2020
Subgridding framework	**0.97**	0.88	**0.71**	**0.98**	**0.52**	**0.87**
HRDPS	0.68	**0.97**	0.43	0.86	0.51	0.46

Table 2. Nash-Sutcliffe model Efficiency coefficient for SWE at each site for each season

lowering with elevation. Second, the aspect gradient is respected with lower incoming shortwave radiations and slightly lower temperatures in the north aspects. Moreover, wind direction is mostly coming from the South, South-West. South slopes are thus more exposed to the wind and north aspects are more sheltered. This is reflected by wind speed values being higher in the south aspects, especially in the alpine. Snow redistribution by the wind is accounted for, leeward slopes getting more snow than windward slopes. Finally, the altitudinal precipitation rate gradient is also respected by the subgridding framework, with precipitation rates getting higher with elevation. This atmospheric parameters variability is then propagated to the modeled snowpacks (Figure 8). Again, the altitudinal gradient in HS is present, with a deeper snowpack from below treeline to the alpine. The wind erosion effect on the snowpack is also well represented, as dominant winds are blowing from the South / South-West. As a result, the south aspect profiles show more defragmented grains (dark green) on the surface and less precipitation particles (lime green), especially in the alpine. On the contrary, the snowpack is deeper in the north aspect because of

https://doi.org/10.5194/egusphere-2023-1152
Preprint. Discussion started: 16 June 2023

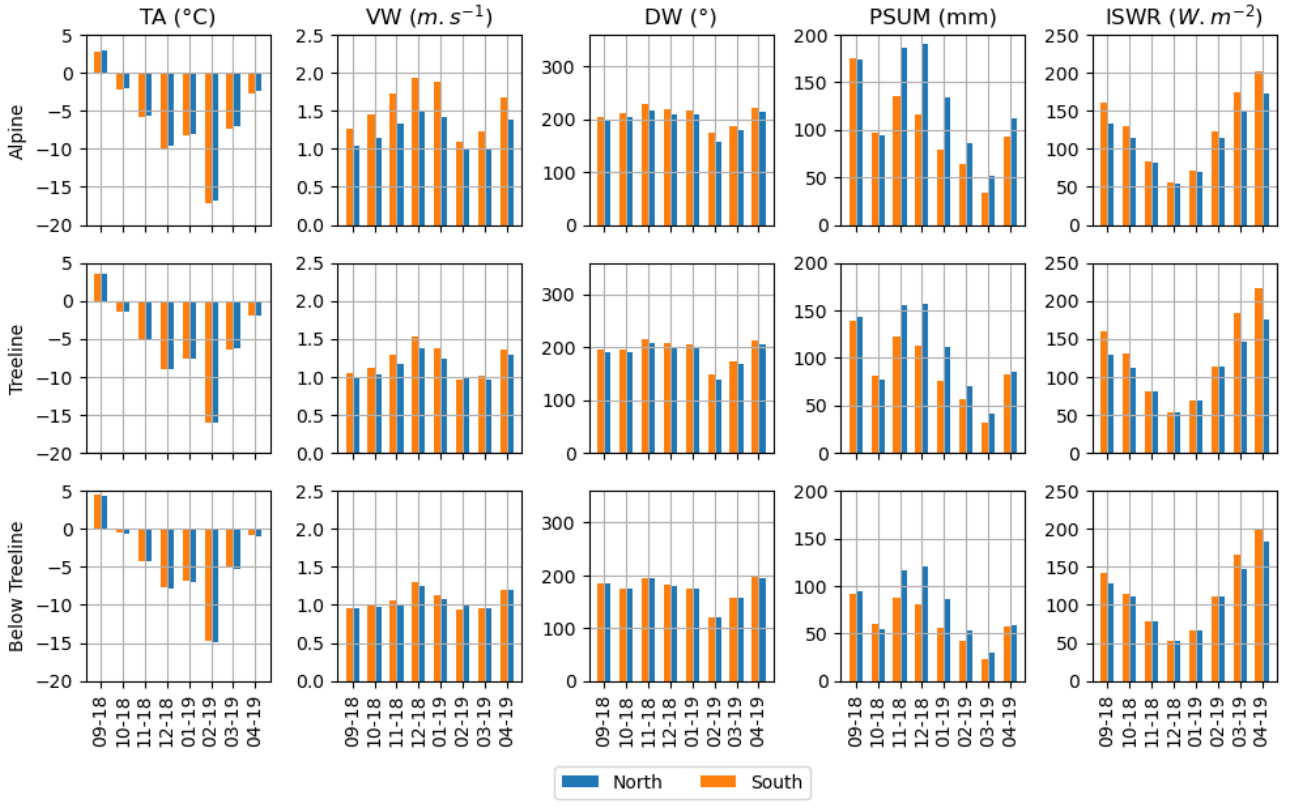

Figure 7. Atmospheric parameters spatial variability assessment for season 2018–2019

snow transport and slower settlement. Finally, the melt onset date is a few days earlier on the south aspect than on the north aspect, and water is percolating faster and deeper in the snowpack on the south aspects.

Season 2019–2020 results for spatial variability appear in Appendix A, Figures A1 and B1. The subgridding framework creates the same altitudinal and aspect gradients, with more precipitations overall, milder temperatures, and stronger wind speeds on average.

5 Discussion

The proposed downscaling framework brings a considerable improvement to modeled atmospheric parameters when compared to station values. Bias and MAE for VW and RH are constantly attenuated. For precipitation, in most cases, bias is corrected but MAE increases. Indeed, even though the model on average underestimates precipitation, major precipitation events are overestimated (Côté et al., 2017). The “one-directional” lapse-rate correction reduces the overall bias by accurately correcting the small and common underestimation errors but accentuates the overall larger and rarer overestimation errors, thus increasing the MAE. We acknowledge that it limits our work, and our lab currently carries out research to produce an adaptative bias

https://doi.org/10.5194/egusphere-2023-1152
Preprint. Discussion started: 16 June 2023

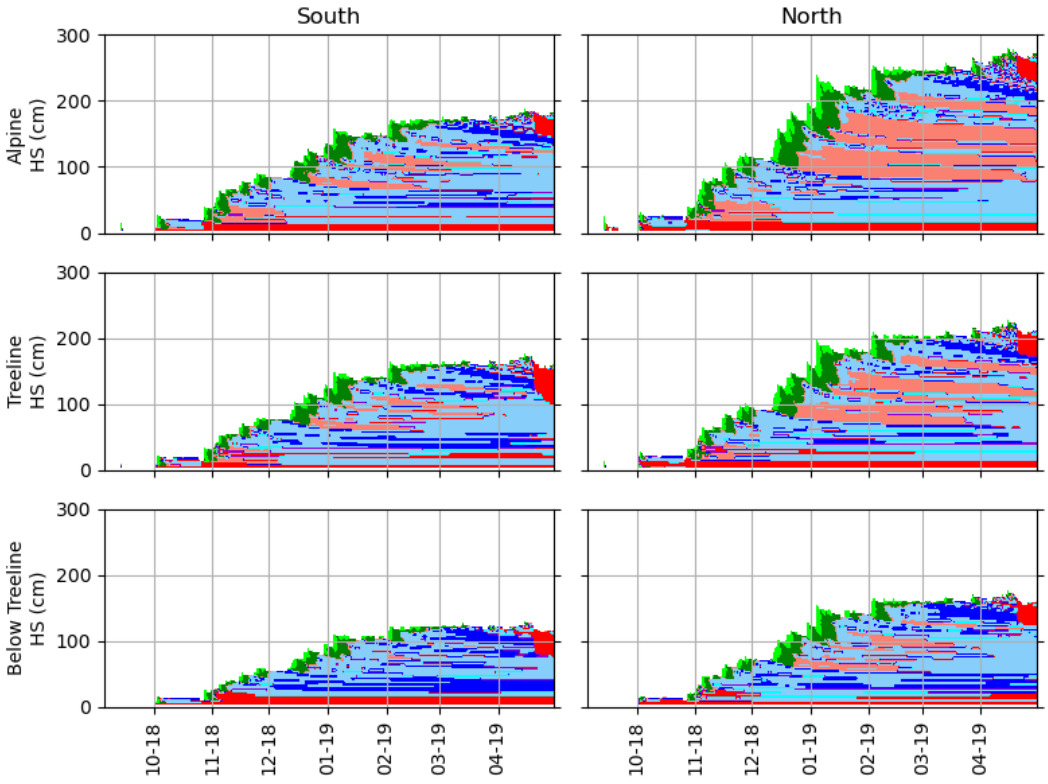

Figure 8. Snowpack spatial variability assessment for season 2018–2019

correction algorithm. Regarding TA, the mean systematic bias is slightly aggravated at every station except at Abbott, where bias is clearly improved. However, the added error remains under 0.5 °C. The same observation can be made about MAE, with the exception being at Hermit, where the MAE slightly lowers (i.e., improved precision). However, TA presents a positive bias at these 3 stations (i.e., HRDPS is colder than station measurements), which are all higher in elevation than the nominal elevation of their corresponding HRDPS cell. As a result, a naive Inverse Distance Weighting lapse-rate spatialization scheme would have introduced even more bias and MAE in the system, aggravating the original error. The logarithmic bias correction reduces the bias in TA. However the IDW spatialization depends on the elevation difference between the HRDPS cell and each sub-pixel. As such, a positive TA bias at the parameterization stage is necessarily aggravated by IDW if the sub-pixel is higher in elevation. Thus, we then argue that the logarithmic lapse-rate parameterization allows reducing the error in the subgridding scheme and keeps it within a physically meaningful interval regarding spatial resolution. Finally, the spatial variability capacity analysis of the subgridding framework shows that our method allows introducing clear and realistic spatial variability, accounting for snow redistribution, topographic effects, and natural elevation or aspect gradients.

The atmospheric parameters subgridding and enhancement directly impacts the quality of the snow simulations, especially on snow height, which is improved at all sites for both seasons (except for Abbott 2019–2020, as explained in section 4.2).

https://doi.org/10.5194/egusphere-2023-1152
Preprint. Discussion started: 16 June 2023

Simulated microstructure parameters are also usually improved, depending on the site and period. The most important errors and lowest similarities occur early in the season, when the snowpack is starting to build. This is due to differences in snow onset timing between simulations and reality, and milder air temperatures early in the season. As a result, there is a fine margin between solid (snow precipitation) and liquid (rain-on-snow), which can strongly alter the microstructure of the snowpack. Moreover, during this period, the snowpack is thinner, and discrepancies between layers have a heavier impact on the mean similarity and mean errors. SWE modeling is overall greatly improved, mainly through the snow height improvement, except at Abbott in 2019–2020 where the error comes from the unusual behaviour of the HRDPS forecast. Furthermore, the subgridding framework allows decreasing by 0.04 mm the OGS overestimation observed with raw HRDPS simulations (averaged over all sites and seasons). However, previous studies showed that SNOWPACK generally overestimates OGS when compared with field observations, even when driven by AWS data (Leppänen et al., 2015; Madore et al., 2018). Thus, the actual error on OGS is likely higher. Finally, the spatial variability of the snowpack properties within one HRDPS cell is achieved; the six profiles show realistic sensitivity to elevation, aspect, and wind exposure. However, wind transport in the alpine is likely exaggerated. This points to the second limitation of our study: the lack of distributed snow validation data, as we only relied on three AWS time series measurements within the study area.

Finally, this work is highly relevant in a remote sensing context. The remote sensing community is currently pushing for new SAR satellite missions, and Observation System Synthetic Experiments have proven that satellite SWE measurements would substantially improve SWE products RMSE (Garnaud et al., 2019; Cho et al., in review, 2022). This study provides finer spatial variability forcing data and improved simulated snowpack state variables regarding NWP driven simulations. As a result, snow simulations performed with such method can provide a realistic first guess estimate of the retrieval parameters, bringing a solid basis to overcome the non-unique solution issue in physical retrieval algorithms (Tsang et al., 2022) and steer away from empirical retrieval approaches. In this context, the next logical step is to design a SWE retrieval algorithm, taking advantage of the vast array of SAR satellites in orbit, such as Sentinel-1 (C-band), TerraSAR-X (X-band), or the SnowSAR mission concept (dual Ku-band) led by Environment and Climate Change Canada and the Canadian Space Agency (Derksen et al., 2021).

6 Conclusions

To the best of our knowledge, this study is the first to focus on downscaling NWP to feed a detailed snow model to improve modeling of both SWE and the microstructural representation of the snowpack over an entire mountainous area. To do so, (i) a new NWP downscaling approach was introduced, by first parameterizing the 2.5 km HRDPS cells into a Virtual Weather Station array, which was then spatially interpolated using the MeteoIO/Alpine3D models. (ii) Snow simulations were performed using the state-of-the-art model SNOWPACK. Microstructure modeling quality was assessed using the DTW algorithm and an original cost function focusing on density and optical grain size, and SWE modeling improvements were quantified using the Nash-Sutcliffe Efficiency coefficient. (iii) Spatial variability of atmospheric parameters and snowpack state variables within one subgridded HRDPS cell was assessed. The main conclusions of this study are:

https://doi.org/10.5194/egusphere-2023-1152
Preprint. Discussion started: 16 June 2023

- The atmospheric parameter subgridding framework yields an overall good performance and introduces a topographically realistic spatial variability. However, research should be carried on to find a more suitable spatialization algorithm for air temperature, and an adaptative precipitation rate correction algorithm.
- This method improves the modeling of the two critical snowpack state variables for snow remote sensing:
  —The general overestimation of OGS by SNOWPACK when driven by raw HRDPS data was decreased by 0.04 mm on average, and up to 0.09 mm.
  —SWE modeling was improved by 17% on average, and up to 41% in the best case.
- In this context, the first three months (September to November) of snow simulations should be considered as a spin-up phase for the snow model, as discrepancies between reality and simulations are critical before the simulations stabilize in December and onward.
- The subgridding framework introduces a realistic spatial variability in the snowpack state variables, respecting altitudinal and orientation gradient as well as ridge effects. Spatial variability is key in SAR remote sensing as it is one the main driver of the backscattering coefficient, especially when multi-looking scenes to a coarser resolution. However, as noted above, the Winstral algorithm may exaggerate the precipitation field altering to represent wind transport.

This study shows that downscaling NWP at a 100 m resolution can improve local representation of atmospheric values and, as a result, improve the snowpack state variables modeling and spatial variability of the snowpack in complex topography. Moreover, the modeling of the two key parameters for snow remote sensing, SWE and OGS, was improved. Future work can thus focus on using these modeled snowpack state variables along with field inferred distributions as a basis for a SWE SAR retrieval algorithm.

Code and data availability. Code and installation guidelines for MeteoIO/SNOWPACK/ALPINE3D can be found at https://gitlabext.wsl.ch/snow-models. The snowpack DTW alignment package can be found at https://CRAN.R-project.org/package=sarp.snowprofile.alignment
Code for the subgridding framework and the data used in this study is available upon request.

Author contributions. PB conceptualized and led the research, wrote the subgridding framework code, did the formal analysis, and wrote the initial draft. AL and BM conceptualized the research, provided scientific inputs, and supervised the project. AL acquired the funding and the resources for the project. All authors reviewed and edited the paper.

Competing interests. Alexandre Langlois is a member of the editorial board of The Cryosphere.

https://doi.org/10.5194/egusphere-2023-1152
Preprint. Discussion started: 16 June 2023

Acknowledgements. This project was funded by the Search and Rescue New Initiatives Fund from Public Safety Canada (SAR-NIF), the Natural Sciences and Engineering Research Council of Canada (NSERC) and the Quebec Research Funds - Nature and Technologies (FRQNT). The authors would like to thank Jeff Goodrich and the Mount Revelstoke and Glacier National Parks staff for their support. The authors also thank Simon Horton and Florian Herla at Simon Fraser University for respectively providing HRDPS data in the .smet format and for onboarding PB in the snowpack DTW package. Finally, the authors thank Nora Helbig and Mathias Bavay for their advice and help with the Alpine3D model.

https://doi.org/10.5194/egusphere-2023-1152
Preprint. Discussion started: 16 June 2023

Appendix A: 2019-2020 spatial variability figures

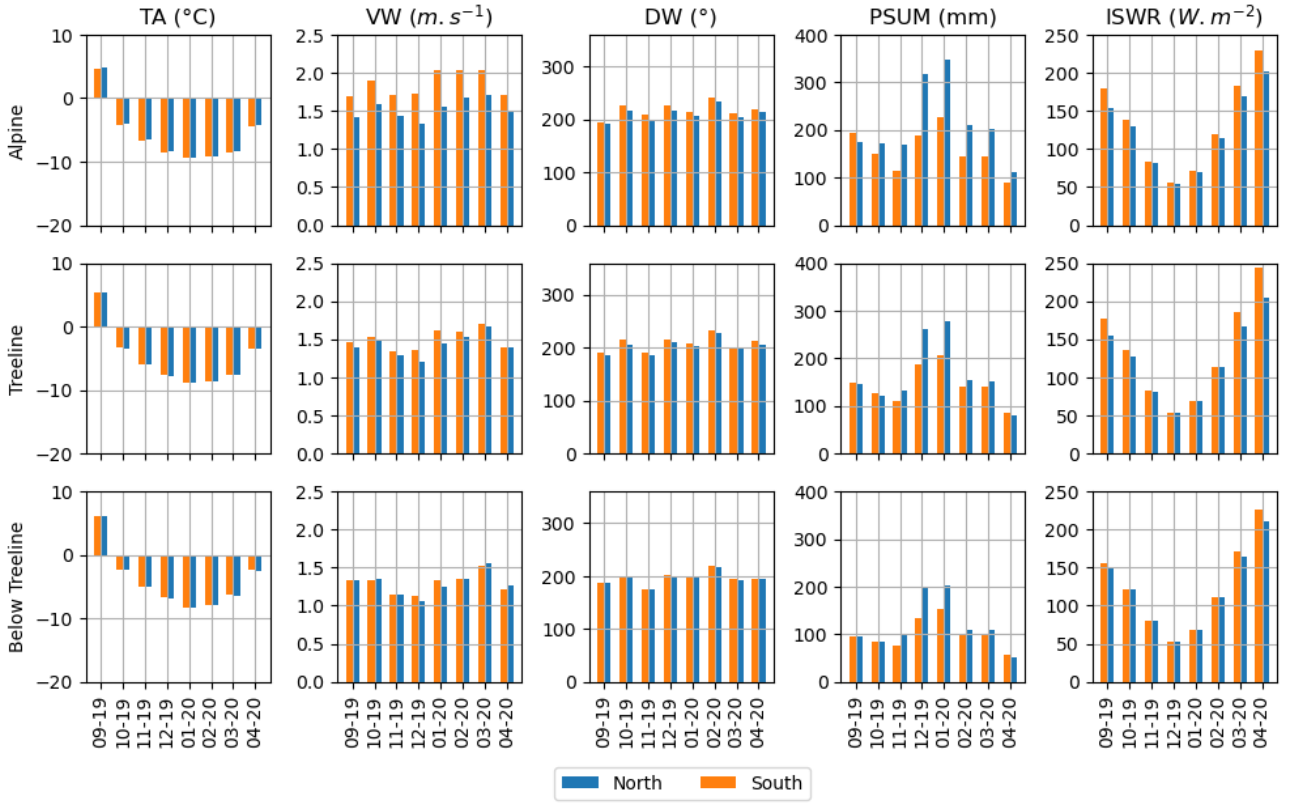

Figure A1. Atmospheric parameters spatial variability assessment for season 2019-2020

https://doi.org/10.5194/egusphere-2023-1152
Preprint. Discussion started: 16 June 2023

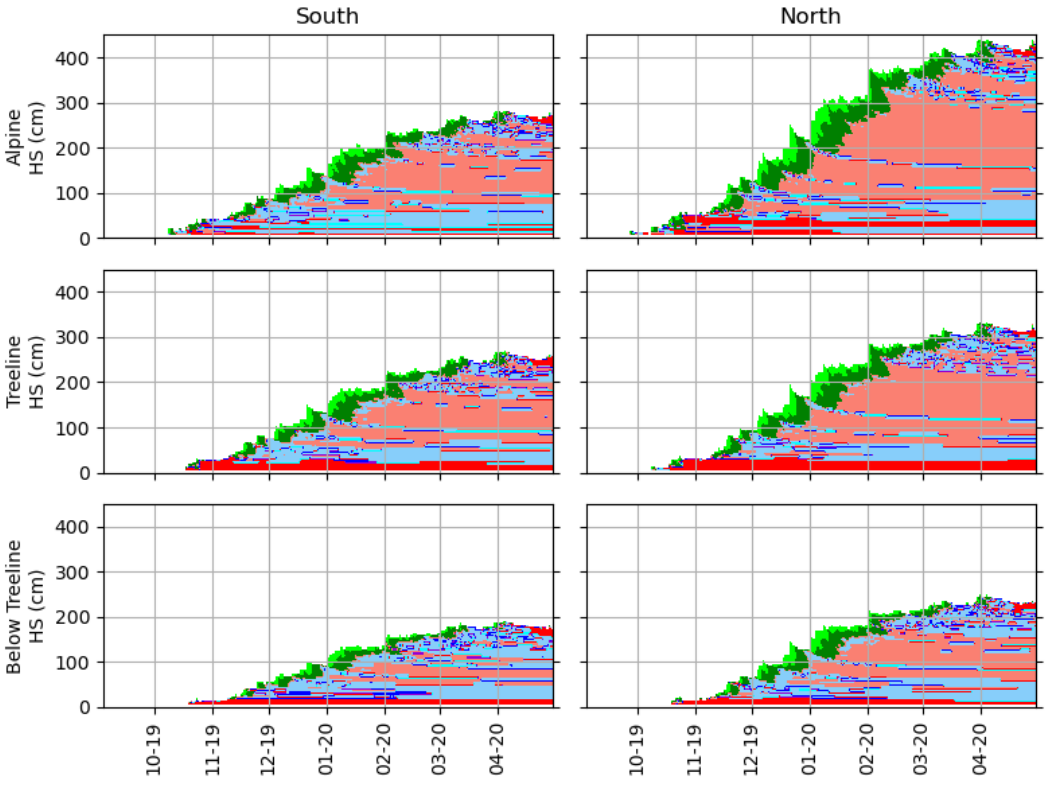

Figure B1. Snowpack spatial variability assessment for season 2019-2020

https://doi.org/10.5194/egusphere-2023-1152
Preprint. Discussion started: 16 June 2023

References

Bartelt, P. and Lehning, M.: A physical SNOWPACK model for the Swiss avalanche warning: Part I: numerical model, Cold Regions Science and Technology, 35, 123–145, https://doi.org/10.1016/S0165-232X(02)00074-5, 2002.

Bavay, M. and Egger, T.: MeteoIO 2.4.2: a preprocessing library for meteorological data, Geoscientific Model Development, 7, 3135–3151, https://doi.org/10.5194/gmd-7-3135-2014, 2014.

Bellaire, S., Jamieson, J. B., and Fierz, C.: Forcing the snow-cover model SNOWPACK with forecasted weather data, Cryosphere, 5, 1115–1125, https://doi.org/10.5194/TC-5-1115-2011, 2011.

Bellaire, S., Jamieson, J. B., and Fierz, C.: Corrigendum to "Forcing the snow-cover model SNOWPACK with forecasted weather data" published in The Cryosphere, 5, 1115–1125, 2011, The Cryosphere, 7, 511–513, https://doi.org/10.5194/TC-7-511-2013, 2013.

Biskaborn, B. K., Smith, S. L., Noetzli, J., Matthes, H., Vieira, G., Streletskiy, D. A., Schoeneich, P., Romanovsky, V. E., Lewkowicz, A. G., Abramov, A., Allard, M., Boike, J., Cable, W. L., Christiansen, H. H., Delaloye, R., Diekmann, B., Drozdov, D., Etzelmüller, B., Grosse, G., Guglielmin, M., Ingeman-Nielsen, T., Isaksen, K., Ishikawa, M., Johansson, M., Johannsson, H., Joo, A., Kaverin, D., Kholodov, A., Konstantinov, P., Kröger, T., Lambiel, C., Lanckman, J.-P., Luo, D., Malkova, G., Meiklejohn, I., Moskalenko, N., Oliva, M., Phillips, M., Ramos, M., Sannel, A. B. K., Sergeev, D., Seybold, C., Skryabin, P., Vasiliev, A., Wu, Q., Yoshikawa, K., Zheleznyak, M., and Lantuit, H.: Permafrost Is Warming at a Global Scale, Nature Communications, 10, 264, 2019.

Brun, E., David, P., Sudul, M., and Brunot, G.: A Numerical Model to Simulate Snow-Cover Stratigraphy for Operational Avalanche Forecasting, Journal of Glaciology, 38, 13–22, https://doi.org/10.3189/S0022143000009552, 1992.

Cho, E., Vuyovich, C. M., Kumar, S. V., Wrzesien, M. L., and Kim, R. S.: Evaluating the utility of active microwave observations as a snow mission concept using Observing System Simulation Experiments, The Cryosphere Discuss. [preprint], https://doi.org/10.5194/tc-2022-220, in review, 2022.

Côté, K., Madore, J.-B., and Langlois, A.: Uncertainties in the SNOWPACK multilayer snow model for a Canadian avalanche context: sensitivity to climatic forcing data, Physical Geography, 38, 124–142, https://doi.org/10.1080/02723646.2016.1277935, 2017.

Derksen, C., King, J., Belair, S., Garnaud, C., Vionnet, V., Fortin, V., Lemmetyinen, J., Crevier, Y., Plourde, P., Lawrence, B., van Mierlo, H., Burbidge, G., and Siqueira, P.: Development of the Terrestrial Snow Mass Mission, in: 2021 IEEE International Geoscience and Remote Sensing Symposium IGARSS, pp. 614–617, IEEE, Brussels, Belgium, https://doi.org/10.1109/IGARSS47720.2021.9553496, 2021.

Dozier, J. and Shi, J.: Estimation of Snow Water Equivalence Using SIR-C/X-SAR. II. Inferring Snow Depth and Particle Size, IEEE Transactions on Geoscience and Remote Sensing, 38, 2475–2488, https://doi.org/10.1109/36.885196, 2000.

Garnaud, C., Bélair, S., Carrera, M. L., Derksen, C., Bilodeau, B., Abrahamowicz, M., Gauthier, N., and Vionnet, V.: Quantifying Snow Mass Mission Concept Trade-Offs Using an Observing System Simulation Experiment, Journal of Hydrometeorology, 20, 155–173, https://doi.org/10.1175/JHM-D-17-0241.1, 2019.

Grünewald, T., Schirmer, M., Mott, R., and Lehning, M.: Spatial and Temporal Variability of Snow Depth and Ablation Rates in a Small Mountain Catchment, The Cryosphere, 4, 215–225, https://doi.org/10.5194/tc-4-215-2010, 2010.

Hagenmuller, P. and Pilloix, T.: A new method for comparing and matching snow profiles, application for profiles measured by penetrometers, Frontiers in Earth Science, 4, 52, https://doi.org/10.3389/FEART.2016.00052/BIBTEX, 2016.

Hagenmuller, P., van Herwijnen, A., Pielmeier, C., and Marshall, H.-P.: Evaluation of the snow penetrometer Avatech SP2, Cold Regions Science and Technology, 149, 83–94, https://doi.org/10.1016/j.coldregions.2018.02.006, 2018.

https://doi.org/10.5194/egusphere-2023-1152
Preprint. Discussion started: 16 June 2023

Helbig, N., Mott, R., Van Herwijnen, A., Winstral, A., and Jonas, T.: Parameterizing surface wind speed over complex topography, Journal of Geophysical Research: Atmospheres, 122, 651–667, https://doi.org/10.1002/2016JD025593, 2017.

Herla, F., Horton, S., Mair, P., and Haegeli, P.: Snow profile alignment and similarity assessment for aggregating, clustering, and evaluating snowpack model output for avalanche forecasting, Geoscientific Model Development, 14, 239–258, https://doi.org/10.5194/GMD-14-239-2021, 2021.

IPCC: IPCC Special Report on the Ocean and Cryosphere in a Changing Climate, pp. 3–35, Cambridge University Press, Cambridge, UK and New York, USA, https://doi.org/https://doi.org/10.1017/9781009157964.001, 2019.

King, J., Kelly, R., Kasurak, A., Duguay, C., Gunn, G., Rutter, N., Watts, T., and Derksen, C.: Spatio-Temporal Influence of Tundra Snow Properties on Ku-band (17.2 GHz) Backscatter, Journal of Glaciology, 61, 267–279, https://doi.org/10.3189/2015JoG14J020, 2015.

King, J., Derksen, C., Toose, P., Langlois, A., Larsen, C., Lemmetyinen, J., Marsh, P., Montpetit, B., Roy, A., Rutter, N., and Sturm, M.: The Influence of Snow Microstructure on Dual-Frequency Radar Measurements in a Tundra Environment, Remote Sensing of Environment, 215, 242–254, https://doi.org/10.1016/j.rse.2018.05.028, 2018.

King, J., Derksen, C., Montpetit, B., and Siqueira, P.: Seasonal Ku-band Radar Measurements across a Snow-Covered Tundra Basin., 76th Annual Eastern Snow Conference, 2019.

Lehning, M., Bartelt, P., Brown, B., Fierz, C., and Satyawali, P.: A physical SNOWPACK model for the Swiss avalanche warning: Part II. Snow microstructure, Cold Regions Science and Technology, 35, 147–167, https://doi.org/10.1016/S0165-232X(02)00073-3, 2002.

Lehning, M., Völksch, I., Gustafsson, D., Nguyen, T. A., Stähli, M., and Zappa, M.: ALPINE3D: a detailed model of mountain surface processes and its application to snow hydrology, Hydrological Processes, 20, 2111–2128, https://doi.org/10.1002/hyp.6204, 2006.

Lemmetyinen, J., Kontu, A., Pulliainen, J., Vehviläinen, J., Rautiainen, K., Wiesmann, A., Mätzler, C., Werner, C., Rott, H., Nagler, T., Schneebeli, M., Proksch, M., Schüttemeyer, D., Kern, M., and Davidson, M. W. J.: Nordic Snow Radar Experiment, Geoscientific Instrumentation, Methods and Data Systems, 5, 403–415, https://doi.org/10.5194/gi-5-403-2016, 2016.

Lemmetyinen, J., Derksen, C., Rott, H., Macelloni, G., King, J., Schneebeli, M., Wiesmann, A., Leppänen, L., Kontu, A., and Pulliainen, J.: Retrieval of Effective Correlation Length and Snow Water Equivalent from Radar and Passive Microwave Measurements, Remote Sensing, 10, 170, https://doi.org/10.3390/rs10020170, 2018.

Leppänen, L., Kontu, A., Vehviläinen, J., Lemmetyinen, J., and Pulliainen, J.: Comparison of traditional and optical grain-size field measurements with SNOWPACK simulations in a taiga snowpack, Journal of Glaciology, 61, 151–162, https://doi.org/10.3189/2015JoG14J026, 2015.

Lievens, H., Demuzere, M., Marshall, H.-P., Reichle, R. H., Brucker, L., Brangers, I., de Rosnay, P., Dumont, M., Girotto, M., Immerzeel, W. W., Jonas, T., Kim, E. J., Koch, I., Marty, C., Saloranta, T., Schöber, J., and De Lannoy, G. J. M.: Snow Depth Variability in the Northern Hemisphere Mountains Observed from Space, Nature Communications, 10, 4629, https://doi.org/10.1038/s41467-019-12566-y, 2019.

Lievens, H., Brangers, I., Marshall, H.-P., Jonas, T., Olefs, M., and De Lannoy, G.: Sentinel-1 Snow Depth Retrieval at Sub-Kilometer Resolution over the European Alps, The Cryosphere, 16, 159–177, https://doi.org/10.5194/tc-16-159-2022, 2022.

Liston, G. E. and Elder, K.: A Meteorological Distribution System for High-Resolution Terrestrial Modeling (MicroMet), Journal of Hydrometeorology, 7, 217–234, https://doi.org/10.1175/JHM486.1, 2006.

Lundquist, J., Hughes, M., Gutmann, E., and Kapnick, S.: Our Skill in Modeling Mountain Rain and Snow Is Bypassing the Skill of Our Observational Networks, Bulletin of the American Meteorological Society, 100, 2473–2490, https://doi.org/10.1175/BAMS-D-19-0001.1, 2019.

https://doi.org/10.5194/egusphere-2023-1152
Preprint. Discussion started: 16 June 2023

Luojus, K., Pulliainen, J., Takala, M., Lemmetyinen, J., Mortimer, C., Derksen, C., Mudryk, L., Moisander, M., Hiltunen, M., Smolander, T., Ikonen, J., Cohen, J., Salminen, M., Norberg, J., Veijola, K., and Venäläinen, P.: GlobSnow v3.0 Northern Hemisphere Snow Water Equivalent Dataset, Scientific Data, 8, 163, https://doi.org/10.1038/s41597-021-00939-2, 2021.

Madore, J.-B., Langlois, A., and Côté, K.: Evaluation of the SNOWPACK model's metamorphism and microstructure in Canada: a case study, Physical Geography, 39, 406–427, https://doi.org/10.1080/02723646.2018.1472984, 2018.

Milbrandt, J. A., Bélair, S., Faucher, M., Vallée, M., Carrera, M. L., and Glazer, A.: The Pan-Canadian High Resolution (2.5 km) Deterministic Prediction System, Weather and Forecasting, 31, 1791–1816, https://doi.org/10.1175/WAF-D-16-0035.1, 2016.

Nash, J. and Sutcliffe, J.: River flow forecasting through conceptual models part I — A discussion of principles, Journal of Hydrology, 10, 282–290, https://doi.org/10.1016/0022-1694(70)90255-6, 1970.

Natali, S. M., Watts, J. D., Rogers, B. M., Potter, S., Ludwig, S. M., Selbmann, A.-K., Sullivan, P. F., Abbott, B. W., Arndt, K. A., Birch, L., Björkman, M. P., Bloom, A. A., Celis, G., Christensen, T. R., Christiansen, C. T., Commane, R., Cooper, E. J., Crill, P., Czimczik, C., Davydov, S., Du, J., Egan, J. E., Elberling, B., Euskirchen, E. S., Friborg, T., Genet, H., Göckede, M., Goodrich, J. P., Grogan, P., Helbig, M., Jafarov, E. E., Jastrow, J. D., Kalhori, A. A. M., Kim, Y., Kimball, J. S., Kutzbach, L., Lara, M. J., Larsen, K. S., Lee, B.-Y., Liu, Z., Loranty, M. M., Lund, M., Lupascu, M., Madani, N., Malhotra, A., Matamala, R., McFarland, J., McGuire, A. D., Michelsen, A., Minions, C., Oechel, W. C., Olefeldt, D., Parmentier, F.-J. W., Pirk, N., Poulter, B., Quinton, W., Rezanezhad, F., Risk, D., Sachs, T., Schaefer, K., Schmidt, N. M., Schuur, E. A. G., Semenchuk, P. R., Shaver, G., Sonnentag, O., Starr, G., Treat, C. C., Waldrop, M. P., Wang, Y., Welker, J., Wille, C., Xu, X., Zhang, Z., Zhuang, Q., and Zona, D.: Large loss of CO2 in winter observed across the northern permafrost region, Nature Climate Change, 9, 852–857, https://doi.org/10.1038/s41558-019-0592-8, 2019.

Pomeroy, J. W., Stewart, R. E., and Whitfield, P. H.: The 2013 Flood Event in the South Saskatchewan and Elk River Basins: Causes, Assessment and Damages, Canadian Water Resources Journal / Revue canadienne des ressources hydriques, 41, 105–117, https://doi.org/10.1080/07011784.2015.1089190, 2016.

Pulliainen, J., Luojus, K., Derksen, C., Mudryk, L., Lemmetyinen, J., Salminen, M., Ikonen, J., Takala, M., Cohen, J., Smolander, T., and Norberg, J.: Patterns and Trends of Northern Hemisphere Snow Mass from 1980 to 2018, Nature, 581, 294–298, https://doi.org/10.1038/s41586-020-2258-0, 2020.

Rott, H., Yueh, S. H., Cline, D. W., Duguay, C., Essery, R., Haas, C., Hélière, F., Kern, M., Macelloni, G., Malnes, E., Nagler, T., Pulliainen, J., Rebhan, H., and Thompson, A.: Cold Regions Hydrology High-Resolution Observatory for Snow and Cold Land Processes, Proceedings of the IEEE, 98, 752–765, https://doi.org/10.1109/JPROC.2009.2038947, 2010.

Sakoe, H. and Chiba, S.: Dynamic Programming Algorithm Optimization for Spoken Word Recognition, IEEE Transactions on Acoustics, Speech, and Signal Processing, 26, 43–49, https://doi.org/10.1109/TASSP.1978.1163055, 1978.

Sturm, M., Goldstein, M. A., and Parr, C.: Water and Life from Snow: A Trillion Dollar Science Question, Water Resources Research, 53, 3534–3544, https://doi.org/10.1002/2017WR020840, 2017.

Tsang, L., Durand, M., Derksen, C., Barros, A. P., Kang, D.-H., Lievens, H., Marshall, H.-P., Zhu, J., Johnson, J., King, J., Lemmetyinen, J., Sandells, M., Rutter, N., Siqueira, P., Nolin, A., Osmanoglu, B., Vuyovich, C., Kim, E., Taylor, D., Merkouriadi, I., Brucker, L., Navari, M., Dumont, M., Kelly, R., Kim, R. S., Liao, T.-H., Borah, F., and Xu, X.: Review Article: Global Monitoring of Snow Water Equivalent Using High-Frequency Radar Remote Sensing, The Cryosphere, 16, 3531–3573, https://doi.org/10.5194/tc-16-3531-2022, 2022.

Viallon-Galinier, L., Hagenmuller, P., and Lafaysse, M.: Forcing and evaluating detailed snow cover models with stratigraphy observations, Cold Regions Science and Technology, 180, 103 163, https://doi.org/10.1016/J.COLDREGIONS.2020.103163, 2020.

https://doi.org/10.5194/egusphere-2023-1152
Preprint. Discussion started: 16 June 2023

Vionnet, V., Brun, E., Morin, S., Boone, A., Faroux, S., Le Moigne, P., Martin, E., and Willemet, J.-M.: The Detailed Snowpack Scheme Crocus and Its Implementation in SURFEX v7.2, Geoscientific Model Development, 5, 773–791, https://doi.org/10.5194/gmd-5-773-2012, 2012.

Vionnet, V., Fortin, V., Gaborit, E., Roy, G., Abrahamowicz, M., Gasset, N., and Pomeroy, J. W.: Assessing the Factors Governing the Ability to Predict Late-Spring Flooding in Cold-Region Mountain Basins, Hydrology and Earth System Sciences, 24, 2141–2165, https://doi.org/10.5194/hess-24-2141-2020, 2020.

Vionnet, V., Marsh, C. B., Menounos, B., Gascoin, S., Wayand, N. E., Shea, J., Mukherjee, K., and Pomeroy, J. W.: Multi-Scale Snowdrift-Permitting Modelling of Mountain Snowpack, The Cryosphere, 15, 743–769, https://doi.org/10.5194/tc-15-743-2021, 2021.

Vuyovich, C. M., Jacobs, J. M., and Daly, S. F.: Comparison of Passive Microwave and Modeled Estimates of Total Watershed SWE in the Continental United States, Water Resources Research, 50, 9088–9102, https://doi.org/10.1002/2013WR014734, 2014.

Winstral, A., Elder, K., and Davis, R.: Spatial Snow Modeling of Wind-Redistributed Snow Using Terrain-Based Parameters, Journal of Hydrometeorology, 3, 524 – 538, https://doi.org/10.1175/1525-7541(2002)003<0524:SSMOWR>2.0.CO;2, 2002.

Wrzesien, M. L., Durand, M. T., Pavelsky, T. M., Kapnick, S. B., Zhang, Y., Guo, J., and Shum, C. K.: A New Estimate of North American Mountain Snow Accumulation From Regional Climate Model Simulations, Geophysical Research Letters, 45, 1423–1432, https://doi.org/10.1002/2017GL076664, 2018.

Zhu, J., Tan, S., Tsang, L., Kang, D.-H., and Kim, E.: Snow Water Equivalent Retrieval Using Active and Passive Microwave Observations, Water Resources Research, 57, https://doi.org/10.1029/2020WR027563, 2021.